Numerical simulations of wind effects on flexible civil engineering structures

Serge Piperno — Pierre-Emmanuel Bournet

CERMICS – INRIA (project Caiman)
2004, route des Lucioles, B.P. 93
F-06902 Sophia Antipolis Cedex
Serge.Piperno@sophia.inria.fr
http://www.inria.fr/cermics/personnel/Serge.Piperno/

ABSTRACT. *In this paper, we present the global set of elements required for the numerical simulation of wind effects on elementary bridge profiles, particularly possible aeroelastic instabilities. We also propose a possible methodology which is based on an efficient coupling algorithm, a finite-element solver for three-dimensional incompressible Navier-Stokes equations in a moving domain and a structural solver. The fluid solver is detailed, the emphasis being put on the ALE formulation. Numerical and experimental results are compared for cases with a structural rigid motion. On a rectangle, numerical simulations for forced oscillation (heaving or rotation) are qualitatively correct, rather inaccurate, but in good agreements with free oscillation numerical simulations though. On an H-shaped section close to the Tacoma Narrows bridge profile, numerical results are both qualitatively and quantitatively very satisfactory and promising.*

RÉSUMÉ. *Dans cet article, nous présentons la problématique globale de la simulation numérique de l'effet du vent autour de profils de pont élémentaires, notamment l'apparition d'instabilités aéroélastiques, et nous proposons une méthodologie qui repose sur trois éléments essentiels : un algorithme de couplage, un solveur en éléments finis des équations de Navier-Stokes tridimensionnelles "incompressible" en domaine déformable et un solveur structure. Le solveur fluide est présenté en détail, notamment son implémentation en formulation ALE. Les résultats numériques et expérimentaux sont comparés sur des cas-tests où la structure est en mouvement rigide. Sur un rectangle, les simulations numériques en mouvement forcé en translation ou rotation donnent des résultats encourageants, assez imprécis, néanmoins cohérents avec des simulations numériques en mouvement libre. Sur une section proche de celle du pont de Tacoma, les résultats sont qualitativement et quantitativement très prometteurs.*

KEY WORDS : *Fluid-structure interaction, wind effects, aeroelastic coefficients, finite elements, ALE formulation, coupling algorithm, torsional flutter, vortex shedding.*

MOTS-CLÉS : *Interaction fluide-structure, effets du vent, coefficients aéroélastiques, éléments finis, formulation ALE, algorithme de couplage, flottement, détachement tourbillonnaire.*

Revue européenne des éléments finis. Volume 8 – n° 5-6/1999, pages 659 à 687

1. Introduction

Aeroelastic instabilities of civil engineering constructions such as suspension high-rise buildings and bridges have been the subjects of many experimental studies (see [WAS 78] for a good collection of references). With the increase in computational power, the numerical simulation of such phenomena is now possible and some preliminary works have already been reported [NOM 92].

In this paper, we present the global set of models, numerical methods and algorithms which are required for the numerical simulation of wind effects on flexible structures. These elements could be compared to those required for experimental simulations in wind tunnels, and our goal is to reproduce experimental results with computational simulations in order to reduce the simulation costs and eventually the design of civil engineering projects.

We propose a possible set of numerical methods and algorithms to obtain efficient and accurate unsteady numerical simulations of aeroelastic instabilities of bluff bodies in a steady wind. The objective of this paper is to present and validate on preliminary simulations a global methodology. This global methodology is based on three main elements, which are the global coupling algorithm, the fluid flow solver and the structural solver. The global resolution is unsteady, no harmonic or modal assumptions are made. The coupling algorithm proposed in this paper was successfully developed for aerodynamic instabilities in compressible flows [PIP 97]. This staggered algorithm, i.e. the fluid and the structure are advanced in time successively and separately, was shown to be very accurate with time steps much larger than those used in this paper. The fluid solver deals with the incompressible Navier-Stokes equations in three dimensions and in a deforming domain. This necessary feature is implemented using an ALE reformulation of an existing code [PAR 92]. The structural solver is very simple, since this paper only deals with rigid sections of cylinders. The structural model itself is elementary (three degrees of freedom for rigid transverse motion of a section).

Our goal here is to numerically reproduce forced oscillation and free oscillation experiments of two benchmark sections: a rectangular cylinder of chord to thickness ratio equal to 4 and a cylinder with a H-section close to the profile of the Tacoma Narrows Bridge. These sections have been chosen because many experimental reports are available [SCA 79, SCA 71, WAS 78, WAS 80]. The simulations have been limited to rigid motions of deck sections to allow quick computations on a typical workstation. For each cylinder and for each type of experience, calculations are led under constant winds and numerical results are then compared with experimental results. The quality of these numerical results as well as their computational cost are discussed.

In Section 2, we present the Fluid-Structure interaction models both from the mathematical and from the experimental point of view. In Section 3, we describe the numerical methods used for the simulation. The flow is solved using a finite-element ALE solver, whereas the simple structural model is integrated using the trapezoidal rule. The coupling staggered algorithm is also given. Then, we report numerical results

for all benchmarks, including forced and free oscillation experiments on the rectangle and H-shaped cylinders.

2. Fluid Structure interaction models

For the purpose of this study, we only consider two-dimensional flexible structures in rigid motion. Such structures play the role of a section of a bridge deck. The global strategy developed here could actually deal with linear (or even non-linear), three dimensional structures in small displacements and deformations. The basic concepts and theories implemented are first described in detail. A state of the art review on fluid-structure coupling experiments in wind tunnels is then presented.

2.1. *Simulation models*

The numerical simulation of flows past oscillating obstacles requires the solution of the Navier-Stokes equations on moving and possibly deforming grids. This involves formal models both for the motion of the structure and for the flow surrounding the body. The coupling between those two models appears in the force term expressing the action-reaction principle between the fluid and the obstacle. Our objective here is to give a short description of the physical models used in this study. For fixed bodies, those models introduce the so-called aerodynamic coefficients: drag, lift and momentum whose definition is given here. When the structure is moving, the aeroelastic analysis first investigated by Scanlan [SCA 71] is commonly used and applied here.

2.1.1. *Governing equations*

The main equations governing the fluid motion are given here as well as the equations governing the mechanical behaviour of the bluff body.

Fluid equations

We consider an external, viscous, incompressible flow around the deck section. Therefore, the three-dimensional fluid domain $\Omega(t)$, depicted in Figure 1, depends on time. During the last few years, direct numerical simulation (DNS) or large eddy simulations (LES) have made significant progress. Turbulence models have also been fully tested under a wide range of flow configurations [TRA 97]. For the particular case of unstructured moving and deforming grids, we need additional, careful spatial and temporal discretization methods, and a robust strategy for constructing dynamic meshes. For that reason, in this first stage we will deal with the laminar unsteady incompressible Navier-Stokes equations in three dimensions:

$$\begin{cases} \dfrac{\partial \vec{\mathbf{u}}}{\partial t} + (\vec{\mathbf{u}}.\nabla)\,\vec{\mathbf{u}} - \nu\Delta\vec{\mathbf{u}} + \nabla p = 0 \\ \nabla.\vec{\mathbf{u}} = 0 \end{cases} \qquad [1]$$

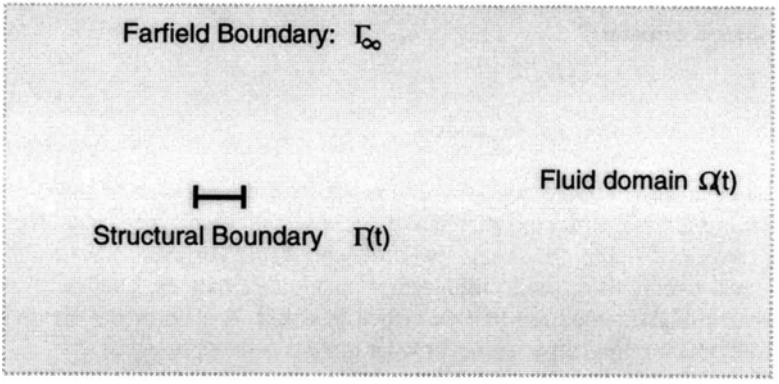

Figure 1. *The time-varying fluid domain* $\Omega(t)$.

where $\vec{\mathbf{u}}$ and p denotes respectively the fluid velocity and the reduced pressure (pressure divided by ρ_F). ν is the kinematic viscosity.

The boundary $\partial\Omega(t)$ is made of two distinct parts: a far field boundary and the deck profile $\Gamma(t)$. Dirichlet type boundary conditions are assumed on both parts of $\partial\Omega(t)$. We set the following boundary conditions:

$$\begin{cases} \text{far field boundary } \Gamma_\infty: & \vec{\mathbf{u}}(t,\vec{x}) = \vec{\mathbf{u}}_\infty \\ \text{structural boundary } \Gamma(t): & \vec{\mathbf{u}}(t,\vec{x}) = \vec{\mathbf{u}}_s(t,\vec{x}) \end{cases}, \qquad [2]$$

where $\vec{\mathbf{u}}_\infty$ is a user set wind velocity (in this case, $\vec{\mathbf{u}}_\infty$ is steady, but could be replaced by a function of the time $\vec{\mathbf{u}}_\infty(t)$ in order to reproduce atmospheric turbulence) and $\vec{\mathbf{u}}_s(t,\vec{x})$ is the structural speed at point $\vec{x}$ and at time t. The second boundary condition is a no slip condition on the fluid-structure interface.

The dimensionalized fluid forces $\vec{F_{\mathbf{F}}}$ per unit surface exerted on the structural surface ($\vec{n}$ denotes the local, external normal to the surface) depend on the pressure and the viscous stress terms.

$$\vec{F_{\mathbf{F}}} = \rho_F \left[-p\vec{n} + \nu \left(\nabla\vec{\mathbf{u}} + \nabla\vec{\mathbf{u}}^T \right) \vec{n} \right]. \qquad [3]$$

Structural model

The structure is a simple bridge deck section (circular, rectangular or H-shaped cylinders) and is assumed rigid. The width D of the section (in the direction orthogonal to the plane of Figure 2 for example) is fixed once and for all. Only two degrees of freedom are given: the vertical displacement y and the rotation θ around the center of rotation (which is also the center of symmetry). Equations for the evolutions of y and θ are written in a dimensional form:

$$\begin{cases} m\ddot{y} + S_\theta\ddot{\theta} + c_y\dot{y} + k_y y &= L_y \\ S_\theta\ddot{y} + I_\theta\ddot{\theta} + c_\theta\dot{\theta} + k_\theta\theta &= M_\theta \end{cases} \qquad [4]$$

where m, I_θ and S_θ denote respectively the mass of the section, and the inertial and static moments of the section around the elastic center; c_y and c_θ are damping coefficients for each degree of freedom, and k_y and k_θ are the corresponding stiffness coefficients. The profile is described on Figure 2. Finally, L_x, L_y and M_θ are the drag,

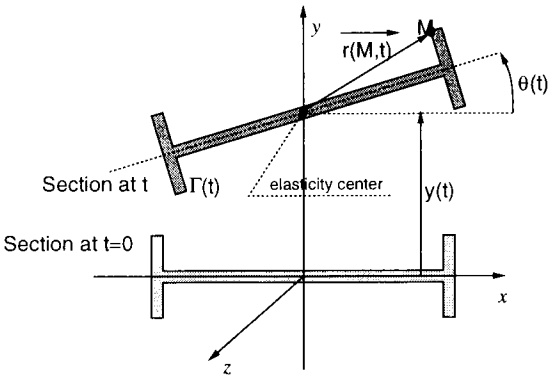

Figure 2. *The two degree-of-freedom deck section.*

lift and moment (around the elastic center) per unit span exerted on the section by the fluid. The fluid force $\vec{F_{\mathbf{F}}}$ (see Eq. [3]) is exerted along the deck profile $\Gamma(t)$. They are then given by:

$$L_x = \int_\Gamma \vec{F_{\mathbf{F}}}.\vec{e_x}\, dl, \quad L_y = \int_\Gamma \vec{F_{\mathbf{F}}}.\vec{e_y}\, dl \qquad [5]$$

$$M_\theta = \int_\Gamma \left(\vec{r} \times \vec{F_{\mathbf{F}}}\right).\vec{e_z}\, dl \qquad [6]$$

where $\vec{r}$ is the location vector taken from the center of elasticity and dl is an element of the contour $\Gamma(t)$.

2.1.2. *Aerodynamic coefficients*

For vortex shedding flows such as those encountered in the aerodynamic analysis of suspension bridges, it is essential to capture correctly the Strouhal number defined by $S = fH/u_\infty$, where f is the dimensional frequency of the vortex shedding and H is a characteristic length scale of the obstacle in the direction perpendicular to the main flow. Vortex shedding is responsible for a periodicity in the pressure field exerted on the structure and accounts for the resulting unsteady forces.

For fixed bodies, the commonly non-dimensional numbers used to characterize the behaviour of a structure submitted to a force exerted by a flow are the drag, lift and

moment coefficients (per unit span). Those unsteady quantities are given by:

$$C_x = \frac{L_x}{0.5\rho_\infty u_\infty^2 B} \; ; \; C_y = \frac{L_y}{0.5\rho_\infty u_\infty^2 B} \; ; \; C_M = \frac{M_\theta}{0.5\rho_\infty u_\infty^2 B^2} \qquad [7]$$

where the density ρ_∞ is the constant density of the incompressible flow, x is the direction of the wind upstream and B is a characteristic length scale of the body in the direction of the wind. As can be seen, the parameters affecting these coefficients are the velocity of the fluid, the size of the bridge, the shape of the bridge, the density of the fluid, and the viscosity of the fluid appearing in the expression of the force.

The drag force appearing in the drag coefficient C_x has several sources: the friction of fluid flowing over the bridge (viscous effects) and the difference in the pressure of the fluid immediately upstream and downstream of the bridge. As the air has a rather low viscosity, in most situations, friction drag remains small compared to pressure drag. Although it is quite small, the friction drag tends to cause a pressure drop behind the bridge, thus increasing the drag component due to pressure effects. It is known that turbulent boundary layers produce more friction and pressure drag than laminar boundary layers. This point will be the object of further investigations. The lift coefficient C_y is the component of the aerodynamic force perpendicular to the wind. This parameter is particularly relevant in wing design. C_M may be interpreted as the capacity of the fluid to make the obstacle rotate. The moment depends on the value of the force, and the arm. Therefore, the value of C_M would vary depending on the chosen arm. In this study, this value is based upon the aerodynamic center (here the geometric center) of the obstacle.

2.1.3. *Aeroelastic analysis*

For the case of moving structures, Scanlan [SCA 71] derived a theory which characterizes the interaction between the flow and the motion of the structure. This theory was guided by the existing works led on airfoils in a classical flutter situation. Basically, the theory assumes linear expressions for the force exerted by the fluid on the structure. The effect of wind on the structure is therefore introduced by the addition, in the structural equations, of rigidity and decay terms which depend on the wind velocity, and which tend, in general, to produce instabilities (flutter, galloping...).
Moreover, the aeroelastic analysis of structures of civil engineering involves a set of aerodynamic data which can only be obtained from wind tunnel experiments.
Generally speaking, the three-dimensional modelling of a given structure requires 2-dimensional aerodynamic data from representative bluff models ("taut-strip models").
In order to cover a wide range of reduced velocity values in the measurement of bridge deck flutter coefficients using a free oscillation method, three vibration regimes were investigated by Scanlan: decaying, steady and diverging. As mentioned before, the study is confined to two-dimensional effects and to a rigid model permitting only two degrees of freedom (see Eq. [4]). The expressions for the lift and moment are simpli-

fied in the following way [SIM 96]:

$$L_y = \frac{1}{2}\rho u_\infty^2 B\left(KH_1^*\frac{\dot{y}}{u_\infty} + KH_2^*\frac{B\dot{\theta}}{u_\infty} + K^2H_3^*\theta + K^2H_4^*\frac{y}{B}\right) \quad [8]$$

$$M_\theta = \frac{1}{2}\rho u_\infty^2 B^2\left(KA_1^*\frac{\dot{y}}{u_\infty} + KA_2^*\frac{B\dot{\theta}}{u_\infty} + K^2A_3^*\theta + K^2A_4^*\frac{y}{B}\right) \quad [9]$$

where ρ is the air density and H_1^*, H_2^*, H_3^*, H_4^*, A_1^*, A_2^*, A_3^*, A_4^* are the flutter derivatives and $K = \frac{B\omega}{u_\infty}$ with ω, the flutter frequency (model response frequency). These sectional equations have also been generalized beyond the section to three dimensions, but this is not necessary in the present two-dimensional context. The theory shows that the most relevant parameters are H_1^*, A_2^* and A_3^*. The H_1^* coefficient represents the response of the vertical motion with torsional motion blocked. It remains negative in the majority of cases. The peaks in H_1^* curves observed in some cases are associated with vortex shedding. The A_2^* coefficient compares the degree for torsional stability with the vertical motion restrained. Its sign reversal observed for the large majority of bridges tested reveals their intrinsic proclivity towards single-degree torsional instability (i.e. torsional mode of instability with negligeable vertical motion present). The A_3^* coefficient accounts for the aerodynamic stiffening effect [SCA 71].

Assuming that the coefficients H_i^* and A_i^* are functions only of the reduced velocity, then, Eq. [4] and [9] hold not only for sinusoidal oscillation, but for more general motions with an exponential term of growth or decay (refer to section 2.2.2).

It is common to consider a given sinusoidal forced oscillation in heaving mode. This simplified approach was chosen for the present study. The expression for the vertical displacement is then:

$$y(t) = Re[y_m \exp(i\omega_m t)] \quad [10]$$

the lift force expressed in Eq. [8] reduces to:

$$L_y(t) = Re[\frac{1}{2}\rho u_\infty^2 B\left(iKH_1^*\frac{y_m\omega_m}{u_\infty} + K^2H_4^*\frac{y_m}{B}\right)\exp(i\omega_m t)] \quad [11]$$

Noting $L_y(t) = \frac{1}{2}\rho u_\infty^2 BRe[(C_{LmR} + iC_{LmI})\exp(i\omega_m t)]$ where C_{LmR} and C_{LmI} are the unsteady non dimensional lift coefficients and combining with Eq. [11] yields:

$$[C_{LmR}, C_{LmI}] = \left[K^2H_4^*\frac{y_m}{B}, K^2H_1^*\frac{y_m}{B}\right] \quad [12]$$

A similar analysis can be done for a forced oscillation under torsional mode. Considering a cylinder subjected to a sinusoidal motion with constant amplitude:

$$\theta(t) = Re[\theta_m \exp(i\omega_m t)] \quad [13]$$

and assuming an expression of the type

$$M_{\theta(t)} = \frac{1}{2}\rho u_\infty^2 B^2 Re[(C_{MmR} + iC_{MmI})\exp(i\omega_m t)] \quad [14]$$

for the moment, one gets:

$$[C_{MmR}, C_{MmI}] = \left[K^2 A_3^* \theta_m, K^2 A_2^* \theta_m\right] \quad [15]$$

2.2. *Wind tunnel tests*

Although CFD techniques have made considerable progress during the last decades, a very important part of aerodynamic research is still based on experiments, particularly in the field of aeroelasticity for civil engineering design. Experimentation often appears to be the only way to have access to some coefficients of the theoretical models. In this section, we give some details concerning the experimental setups and techniques generally used to get the main aeroelastic characteristics of the structure. An overview of the parameters of interest is then presented and some comments on the treatment of the experimental data are provided. Further comments about experimental facilities may be found in [SCA 79], [OTS 74] and [WAS 78].

2.2.1. *Experimental setup and flow conditions*

The models used for wind tunnel experiments are generally sectional models from which surfaces are polished and corners are kept sharp. Two end plates are often attached at both ends of the model to make the flow around the structure as two-dimensional as possible. The scale of the model is typically $1/50$. The model is supported by a couple of springs or by a system of rods associated with an engine. This system is designed to allow forced oscillations of the structure either in heaving or in torsional mode.

The characteristics of the reproduced winds are homogeneous over the whole test section. The Reynolds number does not necessarily correspond to the model dimension due to the fact that keeping the Reynolds number unchanged would require very high speeds. Air is pulled across the model, rather than pushed, to avoid uncontrolled turbulence in the wind. If turbulence is desired, then devices are placed upstream of the model to generate controllable, measurable, and repeatable conditions. In the wind tunnel of CSTB in Nantes [FLA 99], dynamometric balances are used to measure the global efforts on the model. Those measurements are made during a preliminary stage. During the tests, the pressures are recorded at different probes located at the wall around the structure. The facility allows investigation of a set of different configurations including a range of flow velocities, flow incidences and different turbulence levels. Moreover, the structure can be fixed or not. For this latter case, free or forced oscillations (for different magnitudes and at different frequencies) are allowed.

2.2.2. *Determination of the aeroelastic coefficients*

From the pressure field and the knowledge of affected surfaces it is possible to extract the efforts on the body and the corresponding aerodynamic coefficients. For static cases, the aerodynamic coefficients are directly inferred from Eq. [7]. For dynamic cases, two configurations are generally considered:

— in the case of forced oscillations (either heaving or torsional mode), the lift force (respectively the moment) discloses a periodic behaviour from which it is possible to extract the non-dimensional lift coefficients C_{LmR} and C_{LmI} (see Eq. [12]) using a Fast Fourier Transform technique.

— in the case of free oscillations, the most relevant quantity is the total structural energy given by:

$$e(t) = (m\dot{y}^2 + k_y y^2(t))/2 + (I_\theta \dot{\theta}^2 + k_\theta \theta^2(t))/2 \qquad [16]$$

This quantity is discussed in Section 3.2.3. An increase in the total structural energy shows the fluid is able to transfer energy to the structure. This is the case for aeroelastic instabilities (possibly leading to destruction) or limit cycles (possibly leading to early fatigue).

For both cases, Scanlan's coefficients H_i^* and A_i^* are found from the theory developed in Section 2.1.3. To accomplish this, y- or θ- motion is first restrained to 0 in separate experiments. The motion is assumed to have the following expression:

$$y(t) = y_m e^{\lambda t} \sin \omega t \qquad [17]$$

$$\theta(t) = \theta_m e^{\lambda t} \sin(\omega t - \theta_1) \qquad [18]$$

where y_m and θ_m are the amplitudes ; θ_1 is the relative phase and λ is the rate of decay or buildup of the oscillation. Equating separately the coefficients of $\cos \omega t$ and $\sin \omega t$ in Eq. [4] using Eq. [9] and [8] yields expressions for the coefficients H_i^* and A_i^*. Details about this theory as well as the expressions for the coefficients may be found in [SCA 71].

3. Numerical simulations

In this section we first describe the numerical techniques implemented to solve the fluid-structure equations (Section 3.1). Section 3.2 is devoted to some applications of the model to circular, rectangular and H-shaped cylinders.

3.1. *Numerical methods*

We provide here a detailed description of the methods and numerical schemes used in this study.

3.1.1. *Computational coupling of codes*

In most cases, numerical simulations of nonlinear transient aeroelastic problems require the use of partitioned procedures where the fluid and the structure subproblems are solved by different methods. Except for structural models with very few degrees of freedom, the monolithic solution of coupled equations requires the development of case-based procedures, which is not economically manageable. This kind of strong coupling is nevertheless possible in some cases [THO 88]. The most general approach nowadays is to enforce loose coupling, where the coupled system is solved subsystem by subsystem, successively. Some variables on the fluid-structure interface are then transferred directly between codes, or between a coupling master-code and other procedures solving each physical subsystem. In both approaches, some heavy information transfers have to be dealt with.

Both fields of loose coupling algorithms [GUR 89, LES 98, PIP 97, LOH 88] and computational coupling of existing codes, where methods tailored to different mathematical models are implemented, have known an important development in the recent years. These loose coupling approaches allow a maximum of flexibility and efficiency, because existing codes are reused in a really modular way, including possible different time and space discretizations [FAR 98]. At the same time, many works have produced general information transfer libraries for the coupling of existing codes (lighlty adapted to speak common specification) [CIS97, BEC 99, COC97] and even architectures for application development based on object technology (DCOM, CORBA, etc...)

3.1.2. *Structural time-integration*

Most simulations of aeroelasticity phenomena are done with linear or rigid models for the structure, especially for civil engineering applications, where the deformations of the structure are very small. Whether the structural motion is rigid or is decomposed along eigenmodes, the equations of motion for a linear structure can be rewritten into a second order differential equation of the form:

$$M_s\ddot{X} + D_s\dot{X} + K_sX = F,$$

where X is the vector of generalized coordinates (degrees of freedom, or modal coordinates), $\dot{X}$ and $\ddot{X}$ denote respectively the first and second time-derivatives of X, and M_s, D_s and K_s are mass, damping and stiffness generalized matrices. F is the vector of generalized fluid forces.

If X^n, V^n, A^n and F^n are respectively numerical approximates for X, $\dot{X}$, $\ddot{X}$ and F at time $t^n = n\Delta t$, the time-integration of the structure is usually performed using the trapezoidal rule:

$$\left\{\begin{array}{l} X^{n+1} = X^n + \Delta t\frac{V^n+V^{n+1}}{2} \\ V^{n+1} = V^n + \Delta t\frac{A^n+A^{n+1}}{2} \\ M_sA^{n+1} + D_sV^{n+1} + K_sX^{n+1} = F^{n+1} \end{array}\right. \qquad [19]$$

The trapezoidal rule is implicit, second-order accurate, and produces no artificial damping. Although numerical dissipation can be tuned [HIL 77] to be optimal for high frequencies, it can nevertheless pollute numerical results concerning overall physical stability, since numerical dissipation competes with the energy transferred by the fluid to the structure (in the case of the fluid-structure system getting unstable).

3.1.3. *Fluid time and space discretizations*

The fluid equations have to be solved in a moving domain. The most general tools available are based on Arbitrary Lagrangian-Eulerian (ALE) approaches, which can be adapted to finite element methods [DON 82, NOM 92] as well as to finite volume methods [BAT 90]: fluid equations are sort of rewritten in a local moving frame of reference and conservation equilibria on elementary volumes are actually rewritten on elementary moving volumes. However, this kind of method could be quite heavy, compared to simplified approaches like transpiration methods [HUF 93], where only boundary conditions at the fluid-structure interface are modified to take the structural motion into account [CHA 99, MED 99].

In the wide family of three-dimensional finite element Navier-Stokes equations solver, we have chosen to use a hybrid P1-bubble/P1 finite-element solver [PAR 92], originally applied on fixed unstructured tetrahedral meshes, which could be easily transformed into an ALE Navier-Stokes solver (without weak reformulation of Navier-Stokes equations in space-time finite element spaces). This solver is known for its good stability for a rather small number of degrees of freedom [ARN 84]. A compressible solver (specially tailored to low Mach numbers) could be used for the numerical simulations of wind effects on bridge decks. But an incompressible solver could be used as well for other fluid-structure interaction problems, like off-shore and marine structures (deep water riser pipes [WIL 99], pipelines [MAY 99], ships [BER 99]).

On a fixed grid, the momentum conservation equation can be rewritten using the material time derivative of the fluid velocity itself:

$$\frac{d}{dt}\left[\vec{\mathbf{u}}(t,\chi(t))\right] - \nu\Delta\vec{\mathbf{u}}(t,\chi(t) + \nabla p(t,\chi(t)) = 0,$$

where $\chi(t)$ is the Eulerian location of a characteristic curve for the fluid velocity field $\vec{\mathbf{u}}$, i.e. $\chi'(t) = \vec{\mathbf{u}}(t,\chi(t))$. The following time discretization is used: for any point x, we can backtrack over a time step Δt the characteristic curve [PAR 92] ending at x, yielding $\chi_{\Delta t}(x)$. We use a first-order backward Euler implicit scheme, which yields for the momentum and mass conservation equations:

$$\begin{cases} \dfrac{\vec{\mathbf{u}}(t^{n+1},x) - \vec{\mathbf{u}}(t^n,\chi_{\Delta t}(x))}{\Delta t} - \nu\Delta\vec{\mathbf{u}}(t^{n+1},x) + \nabla p(t^{n+1},x) = 0 \\ \nabla\cdot\vec{\mathbf{u}}(t^{n+1},x) = 0 \end{cases} \qquad [20]$$

where Δt is the time step and $t^{n+1} = t^n + \Delta t$. If the only term depending on $\vec{\mathbf{u}}(t^n,.)$ is put on the right hand side, the preceding equation takes the form of a generalized

Stokes problem for the fields $\vec{u}(t^{n+1},.)$ and $p(t^{n+1},.)$. A variational formulation is derived from the generalized Stokes problem [20] and yields a linear system of the form

$$\begin{array}{c} A_h \vec{u}_h^{n+1} + B_h p_h^{n+1} = F_h^{n+1}, \\ B_h^T \vec{u}_h^{n+1} = X_h^{n+1}, \end{array} \qquad [21]$$

where A_h is the symmetric definite positive matrix associated with the elliptic operator $k\mathbb{I} - \nu\Delta$, B_h is the matrix associated to pressure gradients, F_h^{n+1} and X_h^{n+1} are source terms deriving from the explicit term $\vec{u}(t^n,\chi_{\Delta t}(x))$ in Eq. [20] (in the weak variational form, products with test functions are computed using Gauss quadrature formulas over tetrahedra, and x is the Eulerian coordinate of the Gauss points considered) and boundary conditions. The linear system in Eq. [21] is solved with a Uzawa method [PIR 88], where the new linear system on p_h^{n+1} is iteratively solved with a preconditioned conjugate gradient algorithm [CIA 78].

The derivation of an ALE solver of Navier-Stokes equations for an incompressible viscous fluid is very simple. The fluid domain $\Omega(t)$ (see Figure 1) is deforming. Thus its discretization must be modified at each time step. This can be done smoothly and efficiently, by techniques (proposed by Batina [BAT 90] and generalized by Lesoinne and Farhat [LES 93]) deriving from an elastic analogy (details can be found in [PIP 97]).

Equations [20] are purely Eulerian, since the fields $\vec{u}$ and p depend on the coordinate x in the laboratory. The time scheme must be rewritten in moving coordinates ξ linked to the moving grid. For any ξ, i.e. for any grid point, we denote by $x(t^n,\xi)$ its Eulerian position at time t^n. We also replace $z(t,x(t,\xi))$ by $z(t,\xi)$ for any quantity z. Equations [20] can now be rewritten for any ξ as

$$\left\{ \begin{array}{l} \dfrac{\vec{u}\left(t^{n+1},\xi\right) - \vec{u}\left(t^n,\bar{\chi}_{\Delta t}(x(t^{n+1},\xi))\right)}{\Delta t} - \nu\Delta\vec{u}\left(t^{n+1},\xi\right)) + \nabla p\left(t^{n+1},\xi\right)) = 0 \\ \nabla.\vec{u}(t^{n+1},\xi) = 0 \end{array} \right.$$

where $\bar{\chi}(t)$ is now the Eulerian location of a characteristic curve for the flow $\vec{u} - \vec{v}$ (i.e. $\bar{\chi}'(t) = (\vec{u} - \vec{v})(t,\bar{\chi}(t))$), and $\vec{v}$ is the vector field of grid velocities (i.e. $\vec{v}(\xi) = \frac{\partial}{\partial t}x(t,\xi)$). Characteristics based on the field $\vec{u} - \vec{v}$ may seem strange, but the physical meaning is clear: Lagrangian characteristics should be backtracked according to $\vec{u}$, but computational values, which are linked to the grid, travel with the velocity field $\vec{v}$. Thus characteristics in the mixed coordinates are backtracked according to $\vec{u} - \vec{v}$. Indeed, this algorithm yields only a global first-order time-scheme. Improved characteristics and algorithms should be considered to achieve second-order time-accuracy, which could be crucial for the accurate numerical simulation of phenomana like vortex shedding, easily polluted by artificial dissipation.

Again, the term $\vec{u}\left(t^n,\bar{\chi}_{\Delta t}(x(t^{n+1},\xi))\right)$ in the preceding equation, can be considered as a source term in a generalized Stokes problem. We should point out here that all computations, including for this source term, can be done in the mesh configuration at time t^{n+1} (see [PIP 98] for details). The derivation of an ALE solver is now

completed. One time integration from time t^n to time t^{n+1} is done in the following way:
Step 1 - Compute the vector field $\vec{\mathbf{v}}$ of vertex velocities for the current time step,
Step 2 - Update the mesh by moving the grid points,
Step 3 - Update finite element matrices involved in [21] depending on the geometry,
Step 4 - Compute the characteristic term deriving from $\vec{\mathbf{u}}\left(t^n, \bar{\chi}_{\Delta t}(x(t^{n+1}, \xi))\right)$ (again, in the weak variational form, products with test functions are computed using Gauss quadrature formulas over tetrahedra, and ξ is the mixed coordinate of the Gauss points considered). For each mixed coordinate ξ,
Step 4a - Backtrack over Δt the modified characteristic curve $\bar{\chi}$ starting from ξ.
Step 4b - Compute the mixed coordinate $\bar{\xi}$ of the point obtained,
Step 4c - Get the not yet updated value $\vec{\mathbf{u}}(t^n, \bar{\xi})$.
Step 5 - Solve the generalized Stokes problem.

3.1.4. *Coupling algorithm*

The coupling algorithm might be a crucial element for the accurate prediction of the stability or instability of a coupled system. Near the stability limit (flutter in acrospace aeroelasticy, vortex shedding in civil engineering, etc...), the surrounding flow is on the verge of transmitting energy to the flexible structure. Before instability, the flow acts as a damper. Beyond the stability limit, the flow yields what is called negative damping.

An important aspect of the numerical simulation of this kind of phenomenon is that numerical methods produce in general their own artificial numerical damping. Moreover, even if existing accurate methods for the numerical simulation of a fluid and a structure (which individually produce a very weak numerical dissipation) are used, the coupling of such methods can induce an artificial damping, which pollutes the whole simulation and can make the estimate for the stability limit very inaccurate.

In the family of staggered partitioned procedures, some algorithms have been developed [LES 98, PIP 97], which are energy-accurate (i.e. the numerical damping of the coupling algorithm is very small for steady harmonic motions) [PIP 99]. For numerical results presented here where numerical validation was sought, we have used a staggered algorithm (which can be used up to thirty time steps per period of coupled oscillation [PIP 96]) with rather small time steps. The coupled algorithm, for a time integration from time t^n to time $t^{n+1} = t^n + \Delta t$, is the following:
Step 1 - Compute the structural prediction $\tilde{X}^{n+1} = X^n + \frac{\Delta t}{2}\left(3V^n - V^{n-1}\right)$. Then, deduce a prediction for the location of the fluid-structure interface and construct a new mesh by propagating the displacement to internal fluid vertices. Store the grid velocities $\vec{\mathbf{v}}$.
Step 2 - Advance the fluid from t^n to t^{n+1} using the fluid ALE solver. Compute the fluid forces $\vec{F}_{\mathbf{F}}^{\,n+1}$ of [3] on the structure at time t^{n+1} and the corresponding generalized forces $F_{\mathbf{F}}^{n+1}$ given by [5] and [6].
Step 3 - Advance the structure with the trapezoidal rule [19] and with the corrected

forces $F^{n+1} = 2F_{\mathbf{F}}^{n+1} - F^n$.

Note that with this kind of algorithm, the matching condition on the fluid and structural boundaries is relaxed: at the end of the current time step, the fluid boundary matches the second-order accurate prediction $\tilde{X}^{n+1}$, which is slightly different from the result of the structural integration X^{n+1}. This is not the case for all algorithms (see for example [LES 98] for a leap-frog type staggered schemes with enhanced matching properties).

3.2. *Simulation results*

In this section, we review numerical results obtained for a panel of significant test cases. Most cases are indeed two-dimensional, since mainly two-dimensional experimental results only are available. Our really three-dimensional solver is then used in a suboptimal way. We intend to make further validation tests for our code in really three-dimensional configurations, like details at the top of bridges or structures in a surrounding flow. Seeking validation of the global code in fixed grid and for the computation of resulting forces, we first consider fixed cylinders.

We then study the oscillation responses of a rectangle cylinder, both for forced and free oscillations. Numerical and experimental results are compared. Finally, we investigate the aeroelastic response of a simplified Tacoma Narrows Bridge deck for different constant wind speeds.

3.2.1. *Fixed cylinders*

We first consider the unsteady laminar flow of a viscous incompressible fluid past a circular cylinder of radius $R = 1m$. We have used $u_\infty = 1m/s$ and $\nu = 0.01m^2/s$, which sets the Reynolds numbers (based on the diameter $d = 2R$ of the cylinder) to $Re = 200$. Both numerical and experimental results for this test case are reviewed in [LEC 84].

After a transient phase, a periodic vortex shedding appears. The corresponding Strouhal number is defined by $S = fd/u_\infty$. The unsteady lift and drag coefficients (per unit span) are plotted on Figure 3. These adimensional coefficients are given by Eq. [7], taking $H = d$. Classically, f is the frequency f_y of oscillations for the lift coefficient C_y. Numerical results show something commonly observed: the frequency f_x of oscillations of the drag coefficient C_x is approximatively $f_x = 2f_y$.

The numerical results for the fixed circular cylinder are in very good agreement with the results reviewed in [LEC 84]. For several values of the time step Δt, the numerical results for S, as well as the average values and amplitudes for the lift and drag coefficients are reported on Table 1. They are compared with the averages of values reported in [LEC 84]. The values obtained by the fluid solver are in the range of other numerical and experimental values. It can be noticed that the time step Δt has some (limited) influence on numerical results. This is probably due to the method of

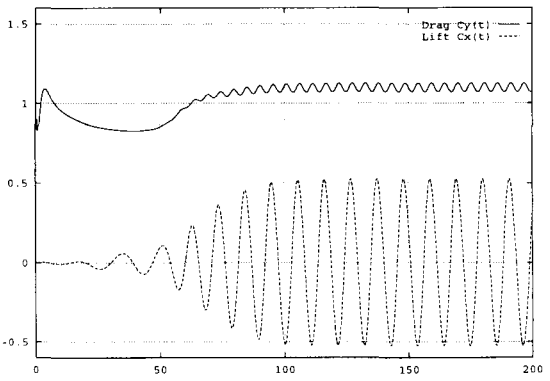

Figure 3. *Lift and drag coefficients (fixed circular cylinder)*

characteristics chosen for the treatment of the non linear advection term. As the time step increases, the second-order error in characteristic curves becomes preponderant.

	C_x	C_y	Strouhal S
$\Delta t = 0.05s$	1.242 ± 0.029	± 0.546	0.188
$\Delta t = 0.10s$	1.253 ± 0.029	± 0.535	0.181
$\Delta t = 0.15s$	1.265 ± 0.028	± 0.518	0.175
Numerics [LEC 84]	$[1.17 - 1.58] \pm 0.04$	$\pm[0.4 - 0.7]$	$[0.15 - 0.194]$
Experiments [LEC 84]	1.30		$[0.16 - 0.19]$

Table 1. *Numerical and experimental S, C_x and C_y (fixed circular cylinder)*

We reproduce the same type of numerical simulations for a fixed rectangular cylinder. We consider a rectangle of chord to thickness ratio B/H equal to 4 (B denotes the chord, the length of the rectangular deck in the direction of the uniform flow, and H is the thickness of the deck in the perpendicular direction). The fluctuation of the flow in the wake behind the stationary rectangle also has a periodic behaviour after a transient phase. The periodic vortex shedding is again characterized by the Strouhal number $S = fH/u_\infty$. We consider experiments with a Reynolds number based on the thickness H $Re \equiv Hu_\infty/\nu = 20000$ ($H = 1m$, $u_\infty = 1m/s$, $\nu = 0.00005$). No turbulence model is used in the computations.

The unsteady lift and drag adimensional coefficients (per unit span) again are given by Eq. [7], with the length c playing the role of D. Again, the shedding frequency f is equal to the frequency of lift oscillations, and equal to the half of the frequency of drag oscillations (see Figure 4). Numerical simulations predict $S = 0.128$, which is in very good agreement with the value given by experiments [OTS 74], which is $S \sim 0.13$.

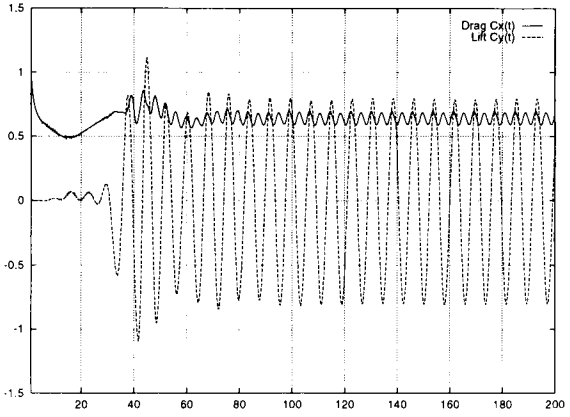

Figure 4. *Lift and drag coefficients (fixed rectangular cylinder with $B/H = 4$)*

3.2.2. *Forced oscillation response of a rectangle cylinder*

We aim at reproducing experimental results reported by Washizu *et al.* [WAS 78]. With numerical simulations of forced oscillations in a heaving mode, we want to study the aeroelastic instability of a rectangle cylinder of aspect ratio equal to 4. The cylinder is given a forced sinusoidal oscillation $y(t) = y_m \cos(\omega_m t)$ and the resulting aerodynamic lift force $L_y(t)$ is computed over a certain number of periods $T_m = 2\pi/\omega_m$. The frequency response part $L_m(t)$ of the signal $L_y(t)$ is defined [OTS 74] by

$$L_m(t) = L_{mR}\cos(\omega_m t) - L_{mI}\sin(\omega_m t),$$

$$\text{with } [L_{mR}, L_{mI}] = \frac{1}{T}\int_{-T}^{T} L(t)[\cos(\omega_m t), -\sin(\omega_m t)]\, dt.$$

The numerical simulation is extended over a great number of periods (typically $T = 30T_m$). It is frequently found convenient to deal with non-dimensional lift coefficients (per unit span) C_{LmR} and C_{LmI} defined by (refer to Eq. [12])

$$\begin{cases} L_{mR} = 0.5\, \rho_\infty u_\infty^2 c\, C_{LmR}, \\ L_{mI} = 0.5\, \rho_\infty u_\infty^2 c\, C_{LmI}. \end{cases}$$

The non-dimensional numbers C_{LmR} and C_{LmI} give information on the effect of aerodynamic forces on the profile, when it is moving in a heaving mode with pulsation ω_m. More precisely, if the coefficient C_{LmR} is positive (respectively negative), the fluid plays the role of an added mass (respectively an added stiffness). The damping effect of the fluid on the structure is directly related to the coefficient C_{LmI}. If $C_{LmI} < 0$, the fluid receives energy from the structure. It plays an actual damping role and the frequency analysis will conclude that the structure is stable. On the contrary, if $C_{LmI} > 0$, the fluid transmits energy to the structure. It is a source of negative damping and the frequency analysis will conclude that the structure is unstable.

The frequency response part analysis can be performed for different values of the amplitude y_m and pulsation ω_m of forced oscillations. The reduced velocity $\mathbf{v}_m = u_\infty T_m/d$ is usually preferred to the dimensional pulsation ω_m. We first report here numerical results for $y_m = 2cm$ and $\mathbf{v}_m$ in the range $[5 : 40]m/s$. The numerical results reported here were obtained after one simulation (with 12 successive periodic regimes and $T = 20T_m$ in each regime) of $60h$ on a Sun Ultra 170 workstation. The computations were made on a 2830-vertex, 7428-tetrahedron unstructured mesh. The three dimensional domain represents a one meter slice around a one meter span section of the rectangular cylinder.

The coefficients C_{LmR} obtained with our ALE fluid solver are compared to those obtained by experiments [WAS 78] on Figure 5. The numerical results for C_{LmR} are

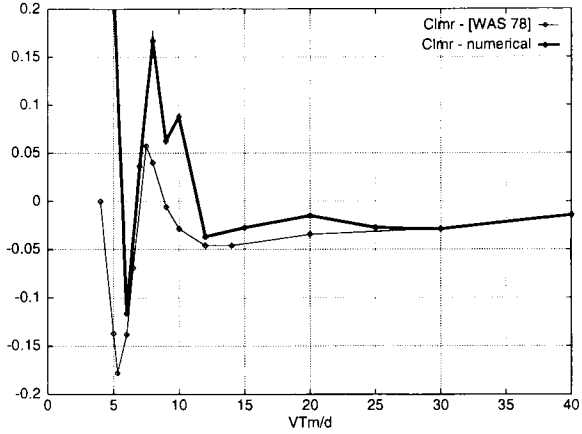

Figure 5. *Coefficients C_{LmR} for $y_m = 2cm$ (numerical simulations and [WAS 78]).*

qualitatively correct. The oscillations in the range $\mathbf{v}_m \in [5 : 10]$ are present, and the behaviour for $\mathbf{v}_m > 25$ is well reproduced. However, the numerical results are far from perfect, since some additional oscillations are present.

For C_{LmI}, the numerical results seem to be shifted in the direction of larger $\mathbf{v}_m$ (see Figure 6). However, both curves give comparable stability results for this rectangular deck in a heaving mode. Experiments predict that the deck is stable for all regimes, the ranges $\mathbf{v}_m < 4$ and $\mathbf{v}_m \in [6 : 7.5]$ excepted, while the present numerical simulation predicts instability in the ranges $\mathbf{v}_m < 6$ and $\mathbf{v}_m \in [7.5 : 12]$. For these simulations, the time step used by the ALE fluid solver was $\Delta t = 0.1s$, which corresponds to fifty time steps per period for the smallest period $T_m = 5$. Thus, the time step does not seem to be at the origin of the $\mathbf{v}_m$ shift between the two curves.

For a larger amplitude $y_m = 10cm$, numerical results for the coefficients C_{LmR} are qualitatively comparable to experiments [WAS 78] (see Figure 7). The oscillations in the range $\mathbf{v}_m \in [5 : 10]$ are again present, and the behaviour for $\mathbf{v}_m > 15$ is well reproduced. However, the numerical results are far from perfect, since the sign of the

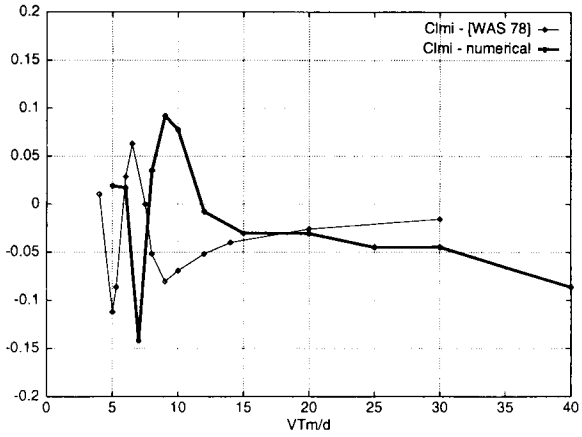

Figure 6. *Coefficients C_{LmI} for $y_m = 2cm$ (numerical simulations and [WAS 78]).*

numerical C_{LmR} is wrong in the range $\mathbf{v}_m \in [6 : 11]$. For the coefficients C_{LmI}, the numerical results are quite accurate (see Figure 8). The dip in the range $\mathbf{v}_m \in [5 : 9]$ is well reproduced, as well as the low frequency behaviour in the range $\mathbf{v}_m < 15$ (however, the computational value for $\mathbf{v}_m = 40$ is suspect). Furthermore, the overall stability of the rectangular cylinder in the whole range $\mathbf{v}_m \in [5 : 40]$ is numerically predicted.

We have also performed numerical simulations of forced oscillations in a torsional mode of the same rectangle cylinder ($B/H = 4$), experiments are reported by Washizu *et al.* [WAS 80]. The cylinder is given a forced sinusoidal oscillation $\theta(t) = \theta_m \cos(\omega_m t)$ and the resulting aerodynamic moment $M(t)$ is computed over a certain number of periods $T_m = 2\pi/\omega_m$. The frequency response part $M_m(t)$ of the

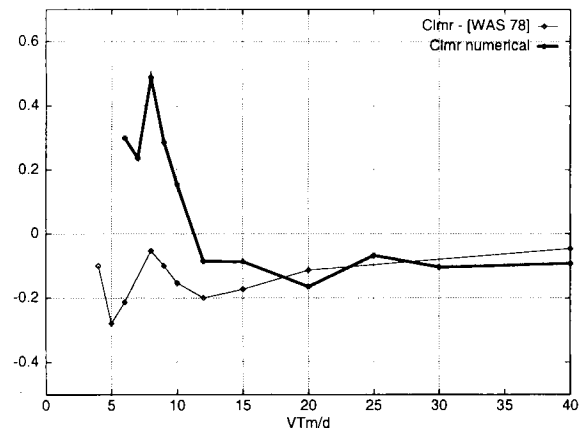

Figure 7. *Coefficients C_{LmR} for $y_m = 10cm$ (numerical simulations and [WAS 78]).*

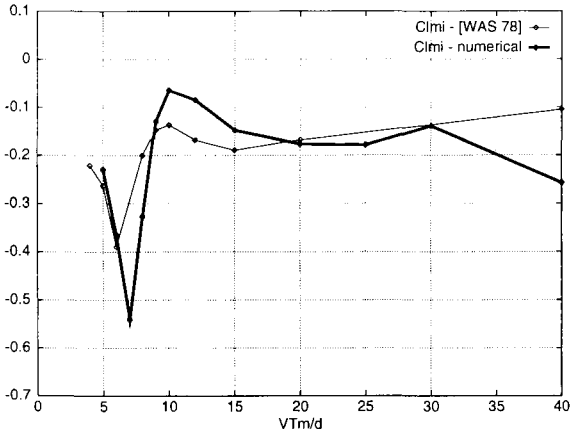

Figure 8. *Coefficients C_{LmI} for $y_m = 8cm$ (numerical simulations and [WAS 78]).*

signal $M(t)$ is defined as previously for $L_m(t)$, yielding the two dimensional quantities M_{mR} and M_{mI}, and eventually the non-dimensional moment coefficients (per unit span) C_{MmR} and C_{MmI} defined by (refer to Eq. [15])

$$\begin{cases} M_{mR} = 0.5\,\rho_\infty u_\infty^2 B^2\, C_{MmR}, \\ M_{mI} = 0.5\,\rho_\infty u_\infty^2 B^2\, C_{MmI}. \end{cases}$$

Again, the non-dimensional numbers C_{MmR} and C_{MmI} give information on the effect of aerodynamic forces on the profile, when it is moving in a torsional mode with pulsation ω_m.

The frequency response part analysis is performed with $\theta_m = 1.91$ deg for different values of ω_m in the range $[5 : 40]$. The numerical results for C_{MmR} are in very good agreement with experiments [WAS 80] (see Figure 9). The dip in the range $\mathrm{v}_m \in [5 : 10]$ is present, and the behaviour for $\mathrm{v}_m > 10$ is very well reproduced.

The numerical results for the coefficients C_{MmI} compare quite well with experiments (see Figure 10). The numerical curve seems slightly shifted in the direction of larger v_m. However, both curves give comparable stability results for this rectangular deck in a torsional mode. Experiments predict the deck is unstable for $\mathrm{v}_m > 20$, while the present numerical simulation predicts instability for $\mathrm{v}_m > 25$. The numerical result for $\mathrm{v}_m \leq 6$ (high frequencies) might be related to a time step $\Delta t = 0.1s$ too large and the result for $\mathrm{v}_m = 40$ is again rather strange. The reader should keep in mind these discrepancies can have multiple origins, lack of turbulence models, computational constraints on the space discretization and the time step Δt to name a few.

3.2.3. *Free oscillation response of a rectangle cylinder*

In this section, we intend to reproduce free oscillation experiments. The rectangle cylinder is given the ability to move freely, but rigidly, in the vertical direction (i.e.

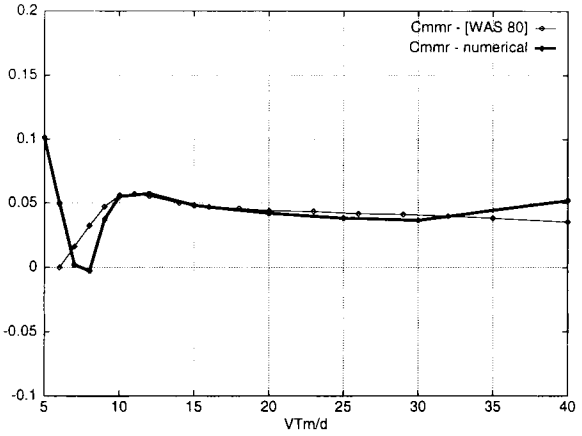

Figure 9. *C_{MmR} for $\theta_m = 1.91$ deg (numerical simulations and [WAS 80]).*

heaving mode). We have noticed that, for forced oscillations at $\mathbf{v}_m = 10$, the fluid has a stabilizing effect for $y_m = 10cm$ and a destabilizing effect for $y_m = 2cm$. We can expect free oscillation experiments to lead to limit cycle oscillations of amplitude between $2cm$ and $10cm$.

We propose a simulation with the following parameters: $B = 4m$, $D = H = 1m$, $u_\infty = 1m/s$, $Re = 20000$ ($\nu = 0.00005$) and, in Eq. [4], $\theta(t) \equiv 0$, $m = 100kg$, $c_y = 0$, $k_y = m\omega_s^2$. The structural pulsation ω_s is taken such that $T_s = 2\pi/\omega_s = 10s$, which yields $u_\infty T_s/H = 10$. The vertical displacement $y(t)$ is forced to $y(t) = y_0 \sin(\omega_s t)$ during ten structural periods T_s. Then the structure is released.

We first test $y_0 = 20cm$. The vertical displacement $y(t)$ is plotted on Figure 11 in function of the time t. When the structure is released after ten periods, the amplitude

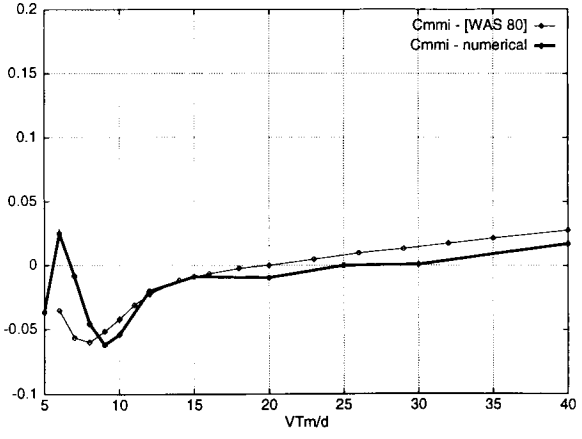

Figure 10. *C_{MmI} for $\theta_m = 1.91$ deg (numerical simulations and [WAS 80]).*

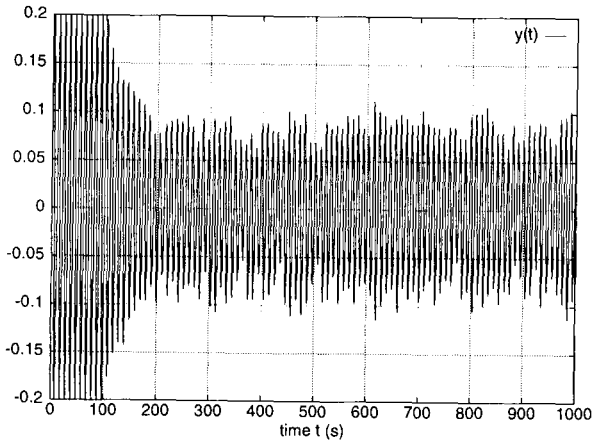

Figure 11. *Vertical displacement for free oscillations ($y_0 = 20cm$, $T_s = 10s$).*

of oscillation decreases and a certain part of the structural energy is transmitted to the fluid. The stabilizing effect of the fluid (in at least the range $y_0 \in [10cm; 20cm]$) is confirmed. After a transient phase, the system evolves in non-periodic pseudo-cycles, where the displacement amplitude is less than $10cm$.

For $y_0 = 5cm$, the amplitude of oscillation increases and a certain part of the structural energy is transmitted by the fluid (see Figure 12). The destabilizing effect of the fluid (in at least the range $y_0 \in [2cm; 5cm]$) is also confirmed. After a transient phase, the system again evolves in aperiodic pseudo-cycles, where the displacement amplitude is also less than $10cm$.

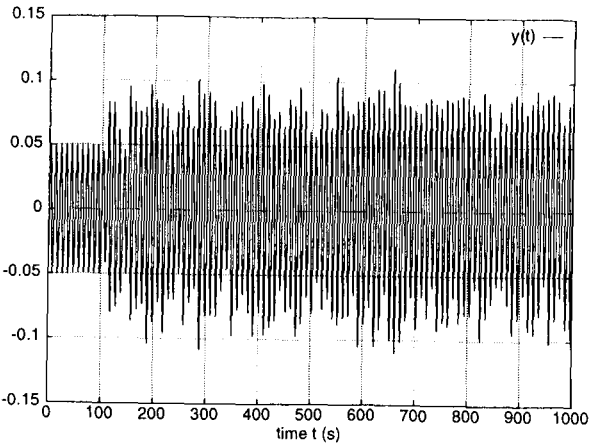

Figure 12. *Vertical displacement for free oscillations ($y_0 = 5cm$, $T_s = 10s$).*

Since the rectangular cylinder is stable for any reduced velocity (see Figure 8) at $y_m = 10cm$, we can reproduce the preceding experience with $y_0 = 10cm$ and different values of T_s in the range $[5 : 40]$. For each T_s, we have plotted on Figure 13 the average structural energy defined by Eq. [16] after a pseudo-limit cycle is obtained. The average energy is of course bounded for all values of T_s. One can notice the strong resonance at $T_s = 10s$. This kind of lock in could be a source of fatigue for flexible structures like a suspended span bridge in a transverse wind.

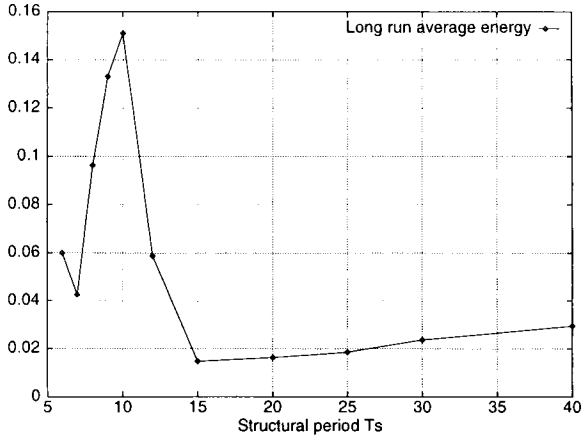

Figure 13. *Long-run average structural energy for free heaving.*

Similar numerical simulations can be performed for free torsional oscillations (rigid motion, with $y \equiv 0$). We now use for the structure: $y(t) \equiv 0$, $I_\theta = 100kg.m^2$, $c_\theta = 0$, $k_\theta = I_\theta \omega_s^2$ in Eq. [4]. For different values of $T_s = 2\pi/\omega_s$ in the range $[5 : 40]$, the rotation $\theta(t)$ is forced to $y(t) = \theta_0 \sin(\omega_s t)$ during ten structural periods T_s (with $\theta_0 = 1.91$ deg), and then the structure is released.

For each $T_s < 15s$, the amplitude of oscillations is bounded. However, as T_s increases, the motion of the rectangle gets less periodic. We have plotted on Figure 14 the average and maximal structural energy (see Eq. [16]) after pseudo-cycles are obtained. The average energy seems constant for $8 < T_s < 15$, but the maximal energy (reached randomly) increases. For $T_s = 15s$, the rotation θ and the energy get unbounded. This kind of lock in could be a source of collapse for flexible structures like a suspended span bridge in a transverse wind. Pressure contours at a time with maximal rotation as the instability develops are plotted on Figure 15. One can notice the darker zone of low pressure under the rectangle, which clearly has a destabilizing effect (the resulting moment $M(t)$ has the same sign as $\theta(t)$).

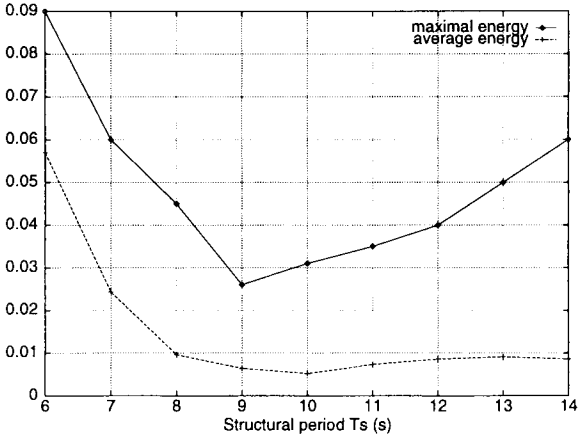

Figure 14. *Long-run average and maximal structural energy for free rotation.*

3.2.4. *The Tacoma Narrows Bridge benchmark*

The first Tacoma Narrows Bridge had an H-shaped cross section that is known to give rise to a phenomenon usually understood as vortex shedding, but more precisely called torsional flutter [SCA 79]. For this kind of H-shaped decks, it has been observed that there is a slight tendency, as the height of the girder is reduced, for more airfoil-like effects to enter. However, for a girder depth as small as 0.1 of the deck width, the tendency to instability remains strong. Scanlan and Tomko concluded that H-sections have very unfavorable aerodynamic stability characteristics [SCA 71].

The bridge collapsed at a critical wind speed of 18.8 m/s, after a support cable at mid-span was snapped by sufficiently large torsional undulations. The modeling of the deck as an H-shaped profile is supported by studies reviewed in [SCA 71]. The approximate geometry of this girder-stiffened type of deck is suggested on Figure 16. We have chosen for the structural geometry and model [TRA 97], the following values:

$$\begin{cases} e_1 = e_2 = 1\ ft = 0.305\ m \\ H = 8\ ft = 2.438\ m \\ B = 39\ ft = 11.887\ m \end{cases}, \quad \begin{cases} m = 8{,}500\ kg/m, \\ I_\theta = 167{,}344\ Kg.m^2/m, \\ k_y = m\omega_y^2, f_y = \omega_y/2\pi = 0.84\ Hz, \\ k_\theta = I_\theta\omega_\theta^2, f_\theta = \omega_\theta/2\pi = 1.11\ Hz, \\ S_\theta = c_y = c_\theta = 0, \end{cases}$$

For the fluid flow, we have tested different values for the wind speed u_∞. We have taken for all computations $\rho_\infty = 1.293\ Kg/m^3$ and $\nu = 1.496\ 10^{-5}\ m^2/s$. The fluid domain around the deck section is discretized by an unstructured mesh of 7,922 vertices and 22,866 tetrahedra. The three dimensional domain again represents a one meter slice around a one meter span section of the bridge. It was built by simple elevation starting from a 3,961 vertex, 7,622 triangle two-dimensional unstructured mesh, which is represented on Figure 17. This mesh is quite coarse (two elements for the discretization of the length e_1 of Figure 16). On this mesh, each of the following

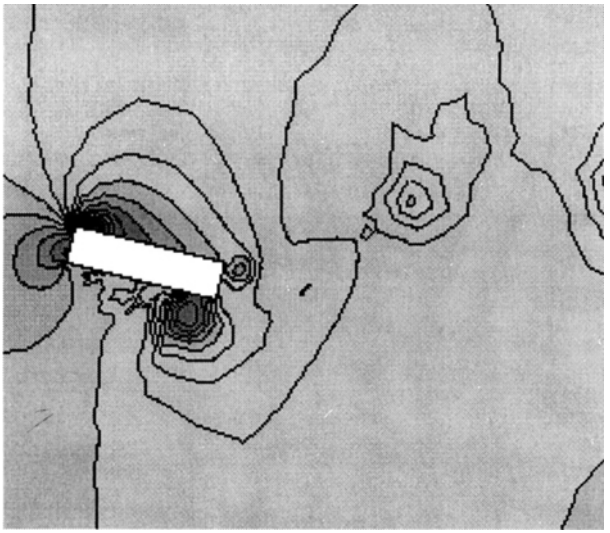

Figure 15. *Pressure contours at maximal rotation for* $T_s = 15$.

30,000 iteration computations required a computational time of four days on a DEC alpha 21164/500.

Numerical results are to be compared with experimental results presented for forced oscillations of the profile [SCA 71]. In this paper, no heaving instability and a torsional instability starting at $V = 28\ ms^{-1}$ are predicted. However, for free oscillation experiments with two degrees of freedom, as the wind speed increases, a heaving instability (induced by vortex shedding) should appear first, then disappear, and finally torsional flutter should take place.

We present here numerical results for free oscillation simulations with several wind speeds V in the range $[20; 40]$. For each test, the total structural energy (see Eq. [16]) is shown on Figure 18 in function of the time. Many conclusions can be drawn from these plots. Some energy is constantly transferred from the fluid to the

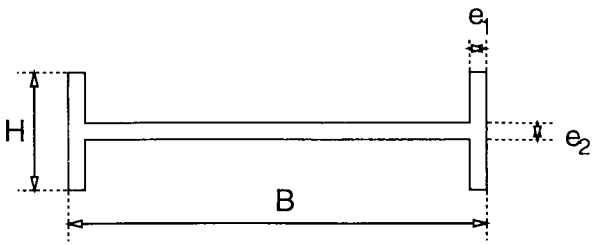

Figure 16. *Approximate geometry of the Tacoma Narrows Bridge deck section.*

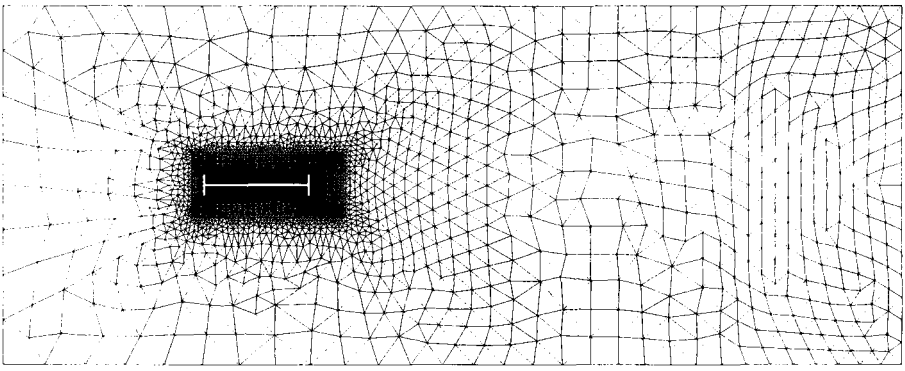

Figure 17. *Discretization of the computational fluid domain.*

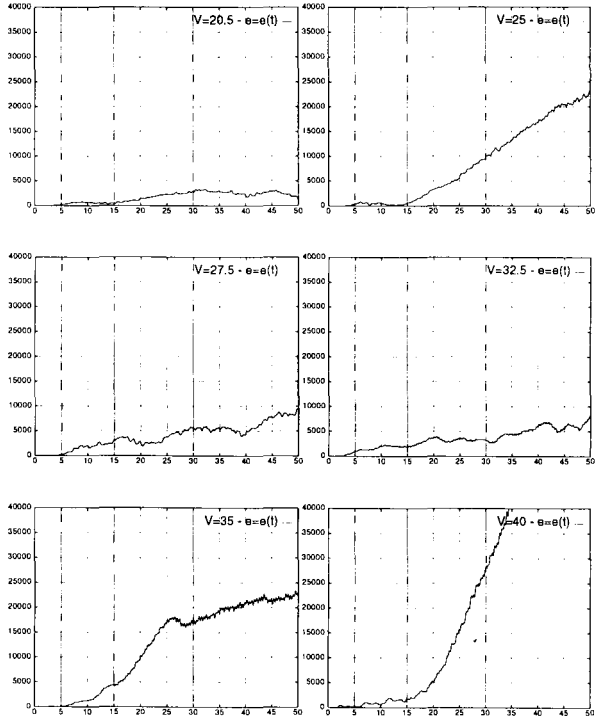

Figure 18. *Total energy for* $V = 20.5\ ms^{-1}$ *to* $V = 40\ ms^{-1}$

structure in some different regimes. An instability is present around $V = 25\ ms^{-1}$, then disappears for larger values of V, then another instability appears for $V \geq 35\ ms^{-1}$. It appears the first instability is purely translational (heaving mode), while the second one is torsional. This is confirmed by plots of the vertical displacement $y(t)$and rotation $\theta(t)$ for $V = 25\ ms^{-1}$ and $V = 35\ ms^{-1}$ (see Figure 19). These conclusions are in very good agreement with experimental results [SCA 71].

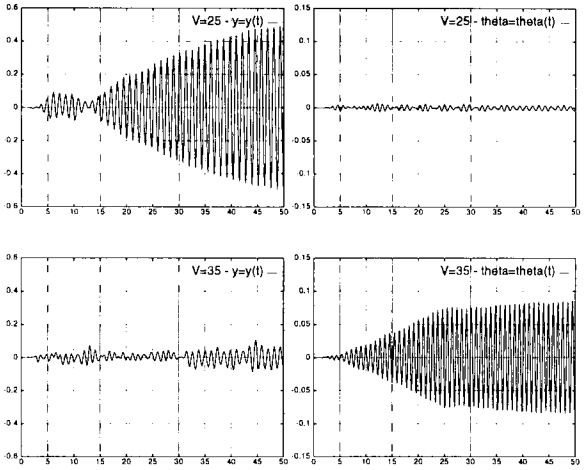

Figure 19. *Displacement and rotation for* $V = 25$ *and* $V = 35$

4. Conclusion

In this paper, we have reported numerical results for the simulation of the interaction of a viscous incompressible flow and rigidly moving sample bridge profiles. We have presented simulations for both forced and free oscillations of the structure. On a rectangular cylinder, numerical results for forced oscillations have yielded satisfactory predictions for the possible instabilities. These predictions include the regime of instability as well as the amplitude in each unstable mode (heaving or torsional). However, the quantitative prediction for the stability limit in terms of the reduced speed $\mathbf{v}_m$ is not very accurate. Free oscillation simulations gave results in very good coherence with forced oscillation simulations for the rectangle cylinder. For an H-section close to the profile of the Tacoma Narrows Bridge, numerical simulations have reproduced the heaving and torsional instabilities of the section, in satisfactory wind speed ranges.

These preliminary results were obtained with no turbulence model, and with an implicit first-order time-scheme which could produce artificial diffusion. Furthermore, the space and time discretizations were rather coarse. All these considerations lead us to be both satisfied with the results obtained and careful. More physical validations

- especially three-dimensional and with flexible structures - are needed to obtain a reliable simulator for this type of fluid-structure interactions. However, numerical simulations of wind effects should now be included in the design process of civil engineering structures. They should at least stand as a valuable complement to wind tunnel experiments in the near future.

Bibliography

[ARN 84] ARNOLD D., BREZZI F., FORTIN M., « A stable finite element for the Stokes equations ». *Calcolo*, vol. 21, n° 4, p. 337-344, 1984.

[BAT 90] BATINA J., « Unsteady Euler Airfoil Solutions Using Unstructured Dynamic Meshes ». *AIAA J.*, vol. 28, p. 1381-1388, August 1990.

[BEC 99] BECKER-LEMGAU U., STECKEL B., TILCH R., « The GRISSLi Coupling Interface for Multi-Disciplinary Simulations and the Twin-Roller Process ». In KVAMSDAL T., ENEVOLDSEN I., HERFJORD K., JENSSEN C. B., MEHR K., NORSETT S. P., Eds., *Computational Methods for Fluid-Structure Interaction, FSI'99*, p. 89-98. Tapir, 1999.

[BER 99] BERGAN P., NESTEGÅRD A., SKEIE G., « Trends in use of computational methods for fluid-structure interactions in the maritime industry ». In KVAMSDAL T., ENEVOLDSEN I., HERFJORD K., JENSSEN C. B., MEHR K., NORSETT S. P., Eds., *Computational Methods for Fluid-Structure Interaction, FSI'99*, p. 197-210. Tapir, 1999.

[CHA 99] CHAPELLE D., FERNÁNDEZ-VARELA M.-A., LE TALLEC P., « Un modèle simplifié d'interaction fluide-structure ». Rapport technique RR-3703, INRIA, June 1999.

[CIA 78] CIARLET P., *The Finite Element Method for Elliptic Problems*. North Holland-Elsevier Science Publishers, Amsterdam, New York, Oxford, 1978.

[CIS97] « CISPAR - open interface for Coupling of Industrual Simulation codes on PARallel computers; ESPRIT Project 20161 ». see http://www.pallas.de/cispar/mhome.htm, 1997.

[COC97] « COCOLIB Deliverable 1.1: Specification of the COupling COmmunications LIBrary; CISPAR ESPRIT Project 20161 ». see http://www.pallas.de/cispar/pages/docu.html, 1997.

[DON 82] DONEA J., GIULIANI S., HALLEUX J., « An Arbitrary Lagrangian Eulerian Finite Element Method for Transient Dynamic Fluid-Structure Interactions ». *Comput. Methods Appl. Mech. Engineering*, vol. 33, p. 689-723, 1982.

[FAR 98] FARHAT C., LESOINNE M., LE TALLEC P., « Load and Motion Transfer Algorithms for Fluid/Structure Interaction Problems with Non-Matching Discrete Interfaces: Momentum and Energy Conservation, Optimal Discretization and Application to Aeroelasticity ». *Comput. Methods Appl. Mech. Engineering*, vol. 157, p. 95-114, 1998.

[FLA 99] FLAMAND O., GRILLAUD G., « Mesure du champ de pression autour de maquettes sectionnelles représentatives de tabliers de ponts ». Rapport technique EN-AEC 99.39 C, CSTB, Nantes, October 1999.

[GUR 89] GURUSWAMY G., « Integrated Approach for Active Coupling of Structures and Fluids ». *AIAA J.*, vol. 27 , p. 788-793, June 1989.

[HIL 77] HILBER H., HUGHES T., TAYLOR R., « Improved numerical dissipation for time integration algorithms in structural dynamics ». *Earthquake Engineering and Structural Dynamics*, vol. 5, p. 283-292, 1977.

[HUF 93] HUFFMAN W., MELVIN R., YOUNG D., JOHNSON F., BUSSOLETTI J. E., BIETERMAN M., HILMES C., « Practical Design and Optimization in Computational Fluid Dynamics ». In *11th AIAA Computational Fluid Dynamics Conference, Orlando, Florida*, July 6-9 1993. AIAA paper 93-3111.

[LEC 84] LECOINTE Y., PIQUET J., « On the use of several compact methods for the study of unsteady incompressible viscous flow round a circular cylinder ». *Comput. & Structures*, vol. 12, n° 4, p. 255-280, 1984.

[LES 93] LESOINNE M., FARHAT C., « Stability analysis of dynamic meshes for transient aeroelastic computations ». In *11th AIAA Computational Fluid Dynamics Conference, Orlando, Florida*, July 6-9 1993. AIAA paper 93-3325.

[LES 98] LESOINNE M., FARHAT C., « A Higher-Order Subiteration Free Staggered Algorithm for Nonlinear Transient Aeroelastic Problems ». *AIAA J.*, vol. 36, n° 9, p. 1754-1756, 1998.

[LOH 88] LOHNER R., « An Adaptive Finite Element Solver for Transient Problems with Moving Bodies ». *Comput. & Structures*, vol. 30, n° 1/2, p. 303-317, 1988.

[MAY 99] MAYER S., HANSEN E., BRYNDUM M., SORTLAND L., VERLEY R., NES H., « KNumerical modelling of pipeline free span vibrations ». In KVAMSDAL T., ENEVOLDSEN I., HERFJORD K., JENSSEN C. B., MEHR K., NORSETT S. P., Eds., *Computational Methods for Fluid-Structure Interaction, FSI'99*, p. 325-336. Tapir, 1999.

[MED 99] MEDIC G., « *Étude mathématique des modèles aux tensions de Reynolds et simulation numérique d'écoulements turbulents sur parois fixes et mobiles* ». PhD thesis, Université de Paris VI, 1999.

[NOM 92] NOMURA T., HUGHES T., « An arbitrary Lagrangian-Eulerian finite element method for interaction of fluid and a rigid body ». *Comput. Methods Appl. Mech. Engineering*, vol. 95, p. 115-138, 1992.

[OTS 74] OTSUKI Y., WASHIZU K., TOMIZAWA H., OHYA A., « A note on the aeroelastic instability of a prismatic bar with square section ». *J. Sound Vibration*, vol. 34, n° 2, p. 233-248, 1974.

[PAR 92] PARES MADRONAL C., « *Etude mathématique et approximation numérique de quelques problèmes aux limites de la mécanique des fluides* ». PhD thesis, Université de Paris VI, 1992.

[PIP 96] PIPERNO S., « Two-dimensional Euler aeroelastic simulations with interface matching relaxation ». In DÉSIDÉRI J.-A., LE TALLEC P., OÑATE E., PÉRIAUX J., STEIN E., Eds., *Proceedings of the Second ECCOMAS Conference on Numerical Methods in Engineering*, p. 898-904, Paris, France, September 9-13 1996. John Wiley & Sons.

[PIP 97] PIPERNO S., « Explicit/Implicit Fluid/Structure Staggered Procedures with a Structural Predictor and Fluid Subcycling for 2D Inviscid Aeroelastic Simulations ». *Internat. J. Numer. Methods Fluids*, vol. 25, p. 1207-1226, 1997.

[PIP 98] PIPERNO S., « Numerical simulation of aeroelastic instabilities of elementary bridge decks ». Rapport technique RR-3549, INRIA, 1998.

[PIP 99] PIPERNO S., FARHAT C., « Partitioned Procedures for the Transient Solution of Coupled Aeroelastic Problems - Part II: Energy Transfer Analysis and Three-Dimensional Applications ». To appear in *Comput. Methods Appl. Mech. Engineering*.

[PIR 88] PIRONNEAU O., *Méthodes des éléments finis pour les fluides*. Collection Recherches en Mathématiques Appliquées. Masson, Paris, 1988.

[SCA 71] SCANLAN R., TOMKO J., « Airfoil and bridge deck flutter derivatives ». *Journal of the Engineering Mechanics Division, ASCE*, vol. 97, n° EM6, p. 1717-1737, December 1971.

[SCA 79] SCANLAN R., « On the State of Stability Considerations for suspended-span bridges under Wind ». In *Proceedings IUTAM-IAHR Symposium*, p. 595-618, Karlsruhe, Germany, 1979.

[SIM 96] SIMIU E., SCANLAN R., *Wind effects on structures*. John Wiley & Sons, New York, London, Sydney, third edition, 1996.

[THO 88] THORNTON E., DECHAUMPHAI P., « Thermal and Structural Analysis of Aerodynamically Heated Panels ». *Journal of Aircraft*, vol. 25, n° 11, p. 1052-1059, 1988.

[TRA 97] TRAN H., KOOBUS B., FARHAT C., « Numerical simulations of vortex shedding flows past moving obstacles using the $k - \varepsilon$ turbulence model on unstructured dynamic meshes ». Rapport technique 97-16, Center for Aerospace Structures, University of Colorado, Boulder, Colorado, October 1997.

[WAS 78] WASHIZU K., OHYA A., OTSUKI Y., FUJII K., « Aeroelastic instability of rectangular cylinders in a heaving mode ». *J. Sound Vibration*, vol. 59, n° 2, p. 195-210, 1978.

[WAS 80] WASHIZU K., OHYA A., OTSUKI Y., FUJII K., « Aeroelastic instability of rectangular cylinders in a torsional mode due to a transverse wind ». *J. Sound Vibration*, vol. 72, n° 4, p. 507-521, 1980.

[WIL 99] WILLDEN R., GRAHAM J., « Numerical simulation of the flow about deep water riser pipes ». In KVAMSDAL T., ENEVOLDSEN I., HERFJORD K., JENSSEN C. B., MEHR K., NORSETT S. P., Eds., *Computational Methods for Fluid-Structure Interaction, FSI'99*, p. 315-324. Tapir, 1999.